GEOPHYSICAL CONSTRAINTS ON MERCURY'S PHYSIOGRAPHIC PROVINCES. Peter B. James[1], Maria T. Zuber[1], Sean C. Solomon[2], Roger J. Phillips[3]. [1]Department of Earth, Atmospheric and Planetary Sciences, Massachusetts Institute of Technology, Cambridge, MA 02139, USA (pjames@mit.edu); [2]Lamont-Doherty Earth Observatory, Columbia University, Palisades, NY 10964, USA; [3]Planetary Science Directorate, Southwest Research Institute, Boulder, CO 80302, USA.

Introduction: Mercury hosts a diversity of physiographic features that distinguish it from the other terrestrial planets. Long-wavelength topography on Mercury is dominated by a number of quasi-linear rises [1], which are associated with thickened crust and are bordered in places by fold and thrust belts. However, at least one rise at 68°N, 32°E, known informally as the northern rise, is not associated with substantially thickened crust [2] or fold and thrust belts. The smooth plains that cover a large fraction of Mercury's surface are mostly interpreted to be volcanic in origin and younger than the surrounding, more heavily cratered terrain [3]. Here we use long-wavelength gravity and topography data provided by the MESSENGER mission to constrain the interior structure associated with specific physiographic regions.

The Mercury Laser Altimeter (MLA) onboard the MESSENGER spacecraft has collected altimetry data [4], and radio tracking has yielded a gravity field to spherical harmonic degree and order 50. These data are mostly limited to the northern hemisphere because of MESSENGER's highly eccentric orbit and northern periapsis.

Localization: Theoretical admittances, Z, and degree-correlations, γ, have been quantified for a number of physical scenarios, [e.g., 5, 6, 7]. Because these theoretical relationships depend on spherical harmonic degree l and may vary spatially, it is necessary to localize gravity and topography in a way that preserves spectral fidelity. Such localization can be accomplished using Slepian tapers, which maximize the concentration of a spherical function's energy within a region while minimizing spectral leakage [8].

There is a fundamental tradeoff between spatial localization and spectral fidelity, which depends on the choice of taper bandwidth. We calculated Slepian tapers with an 8-degree bandwidth, localized within a spherical cap of radius 10° (~440 km). The first zonal taper concentrates 41% of the total energy within 10° and 90% of the energy within 20°. This spatial localization is not ideal, but it limits spectral leakage and allows interpretation of long-wavelength signals.

Uncertainty quantification: Large biases and variances are typically associated with the lowest spherical harmonic degrees of a localized, red-shifted function. Since many of the interesting features on Mercury are associated with low-degree gravity signals, it is important to thoroughly quantify the uncertainties associated with both measurement error and taper variance. We performed an eigenvalue decomposition on the full gravity covariance matrix in order to produce many random realizations of measurement error (we assumed no error in topography). These random errors were applied to the nominal gravity data and localized with Slepian tapers in order to find the resulting distribution of admittances. We multiplied the nominal measurement errors by a factor of 10.

Taper variance arises when a localizing taper variably samples a function at different spherical harmonic degrees. For multi-taper localization of large regions, the taper variance can be estimated with the variance among tapers, but quantifying the effect of this variance for a single taper is more tedious. We estimated single-taper variance by generating many synthetic topography fields with power spectra matching Mercury's power spectrum. We then created synthetic gravity fields by multiplying the topography with a range of admittance spectra proportional to $l^{1.5}$. We applied single Slepian tapers to the north poles of these synthetic topography and gravity fields and calculated the resulting admittances. We then performed a Bayesian likelihood analysis, determining the range of admittances that could produce the observed localized admittance within a confidence interval.

Error ranges in Fig. 1 represent the combined measurement error and taper variance. Confidence intervals of 95% have been used for measurement error and multi-taper variance, whereas single-taper variance was afforded 5 standard deviations.

Interpretation of the results: Spatial variations in admittance and coherence are plotted in Fig. 2 for several spherical harmonic degrees. Admittances and correlations approach zero for degrees above 25 in most locations, likely reflecting the deteriorating quality of gravity data at these short wavelengths. However, gravity and topography can be analyzed at long wavelengths with a higher degree of confidence. We focus on three regions: heavily cratered terrain (HCT), the Caloris basin (28°N, 162°E), and the northern rise.

Heavily cratered terrain. For our purposes we represent the HCT as all area northward of 10°S excluding the northern plains [9] and the Caloris basin and circum-Caloris plains [3]. The quasi-linear topographic rises are mostly contained within the HCT. Low admit-

tances within the HCT imply a shallow depth of compensation, which is consistent with crustal support of topography. However, gravity/topography correlations of less than 0.5 in the HCT suggest that there is some amount of flexural or subsurface loading uncorrelated with crustal thickening [10]. Admittances in the HCT suggest a mean crustal thickness of less than 60 km.

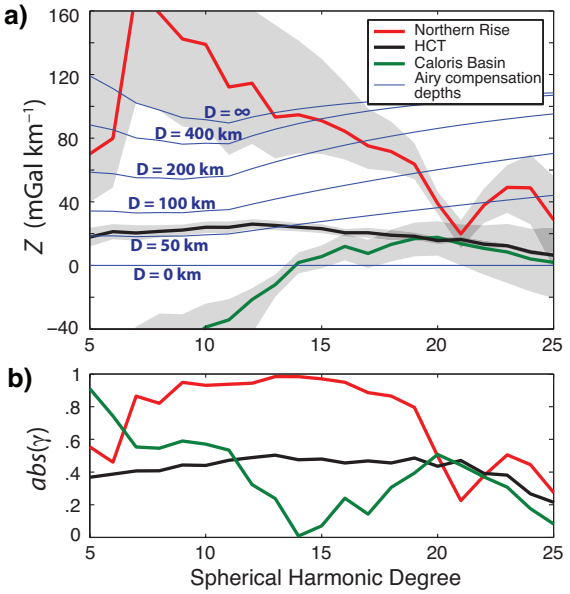

Figure 1. *(a)* Localized 8-degree bandwidth admittances. Blue curves are localized expectations of theoretical Airy admittance. Admittance uncertainties are shaded gray. *(b)* Absolute values of localized coherence.

Caloris basin. We applied a single Slepian taper at the center of Caloris so as to primarily sample the smooth inner plains of the basin. Whereas positive correlations of gravity and topography are expected for crustal compensation of topographic relief, a negative correlation exists within Caloris at the longest wavelengths, similar to the pattern seen for mascon basins of the Moon and Mars. The higher-degree ($l > 20$) admittances and coherences in Caloris and the HCT are comparable (Fig. 1), suggesting similar compensation mechanisms at these length scales.

Northern rise. The northern rise is associated with large admittances and coherences near unity. The admittance spectrum is not consistent with a single compensation depth; admittances at the shortest wavelengths are consistent with crustal (*i.e.,* shallow) compensation, whereas the low-degree admittances suggest a deep compensation mechanism. This contrast is a result of the degree-dependent sensitivity of gravity to mass distributions at different depths.

The predominant compensation mechanism for the northern rise likely is either dynamic flow driven by a mass deficit near the core-mantle boundary [e.g., 7, 11], or flexural stresses in an elastic lithosphere [12]. The admittances associated with deeply compensated topography are similar to the admittances produced by uncompensated topography, so it is difficult to distinguish within error between deep compensation and flexural support of topography.

Conclusions: The northern rise is characterized by uniquely high admittances and correlations, in contrast to the shallow inferred compensation and the poor correlations at the quasi-linear rises. The inner plains of Caloris are compensated differently from the northern volcanic plains, with poor correlation and negative admittances at the longest wavelengths. It remains to be determined whether the negative admittances within Caloris are associated with the basin-forming impact event or with subsequent modification.

References: [1] Byrne P. K. et al. (2012) *LPS,* 43, abstract 2118. [2] Smith D. E. (2012) *Science, 336,* 214-217. [3] Denevi B. W. et al. (2013) *JGR,* submitted. [4] Zuber M. T. et al. (2012) *Science, 336,* 217-220. [5] Turcotte D. L. et al. (1981) *JGR, 86,* 3951-3959. [6] Wieczorek M. A. and Phillips R. J. (1998) *JGR, 103,* 1715-1724. [7] Richards M. A. and Hager B. H. (1984) *JGR, 89,* 5987-6002. [8] Dahlen F. A. and Simons F. J. (2008) *GJI, 174,* 774-807. [9] Head J. W. et al. (2011) *Science, 333,* 1853-1856. [10] Forsyth D. W. (1985) *JGR, 90,* 12623-12632. [11] James P. B. et al. (2012) *LPS, 43,* abstract 2425. [12] Dickson J. L. et al. (2012) *LPS, 43,* abstract 2249.

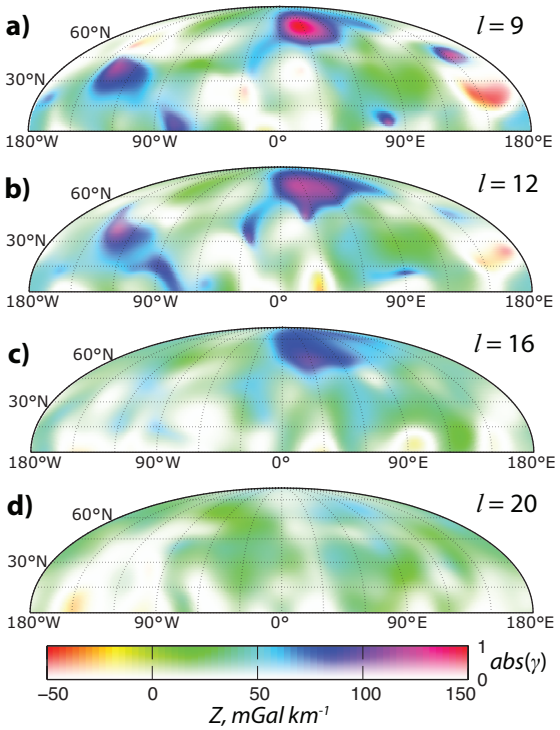

Figure 2. Lateral variation of localized admittance and coherence in Mercury's northern hemisphere, at spherical harmonic degrees $l = 9$, 12, 16, and 20.